Breaking the Diffraction Barrier: Optical Microscopy on a Nanometric Scale

E. BETZIG*, J. K. TRAUTMAN, T. D. HARRIS, J. S. WEINER, R. L. KOSTELAK

In near-field scanning optical microscopy, a light source or detector with dimensions less than the wavelength (λ) is placed in close proximity (<λ/50) to a sample to generate images with resolution better than the diffraction limit. A near-field probe has been developed that yields a resolution of ~12 nm (~λ/43) and signals ~10^4- to 10^6-fold larger than those reported previously. In addition, image contrast is demonstrated to be highly polarization dependent. With these probes, near-field microscopy appears poised to fulfill its promise by combining the power of optical characterization methods with nanometric spatial resolution.

DESPITE THE CURRENT PROLIFERATION of microscopic methods, conventional optical microscopy remains the most widespread imaging technique in use today. This is a consequence of its numerous advantages: it is noninvasive, reliable, fast, inexpensive, easy to use, can be applied to a wide variety of samples, and employs several informative contrast mechanisms. Its primary disadvantage, the limited resolution, has spurred the development of complementary techniques (*1*), but these have always proceeded at the cost of several of these advantages. As a result, there has remained considerable interest in extending the resolution of optical microscopy without a concomitant loss of other attractive features.

Unfortunately, any such efforts that rely on far-field optics will remain wavelength-limited because the propagation of electromagnetic radiation over distances $z > \lambda$ acts as a spatial filter of finite bandwidth (*2, 3*). This results in the familiar diffraction limited resolution of ~λ/2. However, for $z \ll \lambda$, much higher spatial frequencies can be detected since their amplitudes are then of the same order as at the sample ($z = 0$). Consequently, a localized optical probe, such as a subwavelength aperture in an opaque screen, can be scanned raster fashion in this regime to generate an image with a resolution on the order of the probe size. Near-field scanning optical microscopy (NSOM) based on this principle was first proposed by Synge (*4*) and demonstrated at microwave frequencies (λ = 3 cm) by Ash and Nicholls with a resolution of ~λ/60 (*5*).

At visible wavelengths, several different probes have been developed over the last decade that yield superresolution capabilities (*6–16*). Here we report a near-field probe resulting in substantial improvements in resolution, signal strength, and reliability for NSOM. This probe is produced by drawing a single mode optical fiber in a commercial micropipette puller (Sutter Instruments P-87) while heating it with a CO_2 laser. The resulting structure tapers uniformly from the original fiber to a tip having a flat end face perpendicular to the fiber axis. Using angled evaporation, we can coat only the sides with ~100 nm of aluminum (Al), leaving the end face as a transmissive aperture. The tip size can be adjusted easily and reproducibly to produce apertures from <20 nm to >500 nm in diameter. Using higher heat or pulling force, we may be able to make even smaller tips, but below 20 nm, the resolution should be limited by the penetration of the electromagnetic field into the Al coating.

The key to the success of our probe lies in its ability to deliver light efficiently to the aperture. Most efforts to improve NSOM have concentrated on the aperture itself (*6–9*), even though the greatest loss typically occurs within the tapered shank due to retroreflection of the majority of the incident light and absorption of much of the remainder within the walls. By forming the probe from an adiabatically tapered single-mode fiber, we ensure that all the radiation remains bound to the core until a few microns from the tip. Thus, the intensity at the aperture relative to that at the side walls is vastly greater than in earlier tapered probe designs (*7, 9*), resulting in much larger signals and, by virtue of the elimination of background light, better resolution and reliability.

An example of this improved resolution is given in Fig. 1. A test pattern was prepared that, as demonstrated by the electron micrograph in Fig. 1A, consists of 500 nm tall Al letters on a glass substrate. The conventional optical image in Fig. 1B approaches the best resolution obtainable by far-field methods, yet clearly conveys little information at the length scales of interest. In contrast, features are visible in an NSOM image of a similar pattern (Fig. 1C) with dimensions small compared with even the letters themselves.

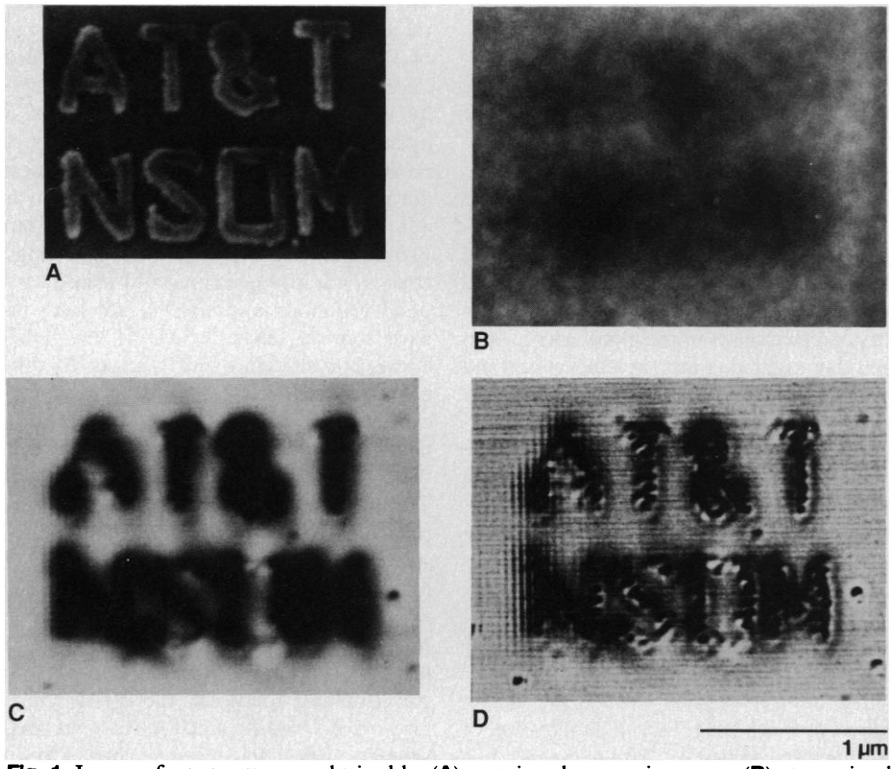

Fig. 1. Images of a test pattern as obtained by (**A**) scanning electron microscopy; (**B**) conventional optical microscopy (100×, 0.9NA objective in transmission); (**C**) NSOM (unprocessed, λ = 514.5 nm); and (**D**) NSOM (after Fourier deconvolution). Vertical lines at the left of (**C**) and (**D**) are artifacts caused by high speed scanning. The frame time was 1 s.

AT&T Bell Laboratories, 600 Mountain Avenue, Murray Hill, NJ 07974.

*To whom correspondence should be addressed.

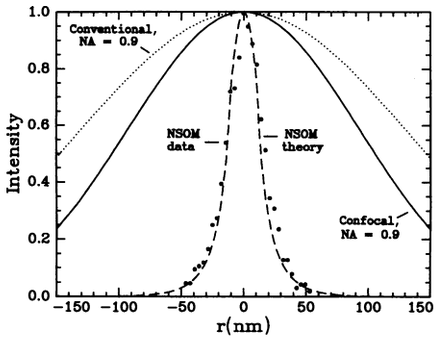

Fig. 2. Comparison of impulse response functions for various optical systems at $\lambda = 514.5$ nm.

Such features are still more pronounced after processing the NSOM data (Fig. 1D) in a manner to be described below.

From such results, it is possible to quantitatively characterize the spatial resolution obtainable with our new probes. The issue of resolution in NSOM is a complicated one, since it is strongly influenced by factors such as polarization and perturbations of the probe field caused by the sample itself (see Fig. 4). Previously adopted criteria include examining the image for the smallest apparent structures observed (*7, 11*) or using test gratings (*12, 14*). The first methods yields ~7-nm resolution versus ~20 nm for the best claim elsewhere (*11*). This is overly optimistic, however, because it neither distinguishes real features from artifacts, exemplary noise or probe scraping, nor recognizes that nonlinear effects, such as from the breakdown of Kirchoff boundary conditions (*17*) or the coupling of vertical evanescence information to the lateral plane, can cause the signal to change on a scale smaller than that of the true structure. The grating criterion is more definitive because it relates NSOM data to specific features as determined by a different, well-established technique. However, only the maximum detectable spatial frequency is thereby determined, whereas any microscope acts as a filter which should be characterized at all frequencies.

Such a characterization can be achieved by using a test object containing all spatial frequencies in equal measure (that is, a delta function). The resulting image is the impulse response function and its Fourier transform yields the transfer function. A comparison of various optical ($\lambda = 514.5$ nm) response functions is presented in Fig. 2. The outer two curves give the theoretical optimum response functions for conventional and confocal systems at a numerical aperture (NA) of 0.9, representing the best possible far-field results without resorting to oil immersion (*18*). Isolated Al particles remaining on the patterns in Fig. 1 after fabrication permitted the NSOM response function to be estimated (third curve, inverted and normalized for comparison). The agreement with a theoretical model of the intensity from a 20-nm aperture in an Al film, determined by treating the aperture as a waveguide with a complex dielectric coefficient in the cladding, is quite good. The data yields a full-width-at-half-maximum of 30 nm, and the transfer function becomes shot noise dominated at a maximum spatial frequency corresponding to ~12-nm resolution (~λ/43), versus ~80 nm for the best grating based claim (*14*). Taking into account the finite sizes of the Al particles can only serve to improve our claim. Thus, the resolution obtained with our new probes is well in excess of that claimed elsewhere, regardless of criterion.

A direct demonstration of our ability to detect high spatial frequencies is provided in Fig. 3. The pattern in this case nominally consists of 50-nm boxes and 100-nm spaces forming a two-dimensional grid, but actually varies as shown in the electron micrograph (Fig. 3A). Since it contains no propagating spatial frequencies, the pattern appears uniformly gray within each box in a conventional optical micrograph (Fig. 3B). On the other hand, the grid structure is clearly evident in the NSOM image (Fig. 3C) of a similar pattern, and even more so in a processed version (Fig. 3D). The largest fundamental spatial frequency is $\sqrt{2}/150$ cycles per nanometer, yielding at least 53-nm resolution. Higher order frequencies are clearly detected as well, but we have thus far been unable to produce grids sufficiently fine to seriously challenge the resolution capabilities of our new probes.

One advantage of the response function is that, in a linear, space-invariant system, it can be used to reconstruct the object by accounting for the spatial filtering properties of the microscope (*2*). Unfortunately, owing to the tip-sample interaction, neither of these requirements is met in NSOM. Nevertheless, one can perform a Fourier deconvolution with the known NSOM response function to arrive at a reconstruction that highlights features in a manner which, while not entirely accurate, is at least not completely ad hoc. Such a procedure was used to generate Figs. 1D and 3D. Many features are much clearer in these images than in their unprocessed counterparts, such as the individual Al grains within the letters in Fig. 1. Careful inspection of electron micrographs also reveals these grains, although they are accentuated in the NSOM case by the aforementioned nonlinear effects.

An oft neglected issue in NSOM is that of signal strength. However, improved resolution at the expense of signal is at best a Pyrrhic victory, because many of the appli-

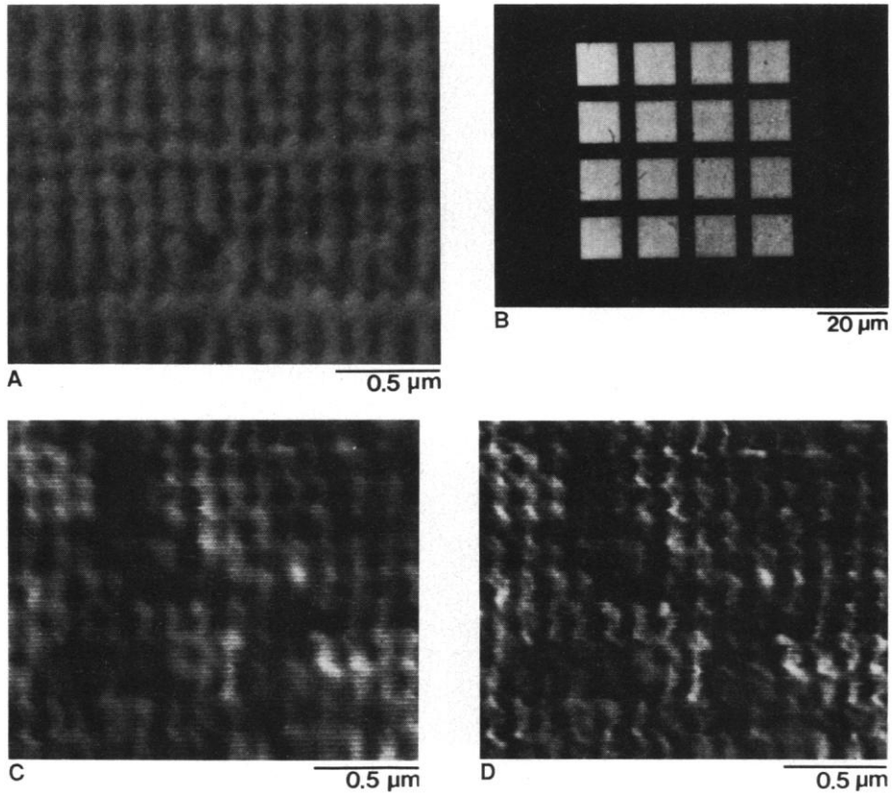

Fig. 3. Images of a periodic pattern with only optically evanescent spatial frequencies as viewed by: (**A**) scanning electron microscopy; (**B**) conventional optical microscopy; (**C**) NSOM (unprocessed); and (**D**) NSOM (after deconvolution).

cations to which NSOM is best suited also benefit from a large photon flux or high collection efficiency. Using an 80-nm aperture in a tapered fiber probe, we have imaged patterns such as those in Fig. 1 with intensities as high as $\sim 1.2 \times 10^{11}$ photons per second (~50 nW), representing gains of $\sim 10^6$, $\sim 10^5$, and $\sim 10^4$, respectively, over the excitonic aperture (*19*), quartz tip (*7, 11*), and pipette (*9, 10, 12, 14*) methods reported previously. Our signals are currently of such magnitude that almost any application originally conceived for far-field optics can now be extended to the near-field regime, including: dynamical studies at video rates and beyond; low noise, high-resolution spectroscopy (also aided by the negligible auto-fluorescence of the probe); minute differential absorption measurements; magnetooptics; and superresolution lithography.

An example illustrating the advantages of and problems inherent in adapting optical contrast mechanisms to NSOM is shown in Fig. 4. Retardation plates placed before the fiber allowed the polarization at the probe tip, as measured in the far-field, to be set to any desired elliptic state. Linear states oriented horizontally (designated probe −) or vertically (probe |) to the letters were chosen for the purposes of Fig. 4. A polarizing film placed immediately before the detector permitted selection of either the horizontal (detector −) or vertical (detector |) field component after transmission through the sample. The images in Fig. 4, which were all taken with the same probe and on the same pattern, clearly demonstrate the ability to highlight specific sample features with polarization NSOM.

At least two distinct contrast mechanisms are involved in the images of Fig. 4. When the probe and detector states are orthogonal (Fig. 4, B and C), the required boundary condition (electric field perpendicular to the pattern edges) causes partial rotation of the polarization. Not surprisingly, this process is most efficient for structures midway between the two states and much less so for those aligned along either axis. On the other hand, when the probe and detector states are parallel (Fig. 4, A and D), lines along the field are wide and dark while those orthogonal to it are narrow and even brighter than the background. Presumably, in the first instance the difficulty of simultaneously satisfying the conflicting boundary conditions at the tip and sample results in a sharp intensity reduction even when the two are only in close proximity to one another. In the latter case, the boundary conditions are more easily satisfied for the combined system than for the tip alone, resulting in enhanced transmission when the aperture is larger than the linewidth.

All the above images were taken in illumination mode, in which light sent down the fiber and emitted by the aperture is collected with an objective after transmission through the sample (*16*). We have recently obtained similar resolution with our tapered fiber probes operating in the reverse configuration, known as collection mode (*12, 16*). In addition, we have imaged other samples including phase objects, luminescent patterns, and magnetic domains with comparably large signals and high resolution. It may be possible to increase the signal beyond $\sim 10^{11}$ photons per second, since the throughput is a strong function of the taper angle as well as the aperture size. On the other hand, our current resolution of ~12 nm (at $\lambda = 514.5$ nm) approaches the limit imposed by the penetration of evanescent fields within the Al film. With our tapered fiber probes, the quantity and diversity of applications accessible to NSOM has expanded, possibly including areas such as immunofluorescence studies of biological systems, spectroscopy of semiconductor microstructures, and optical surface modification.

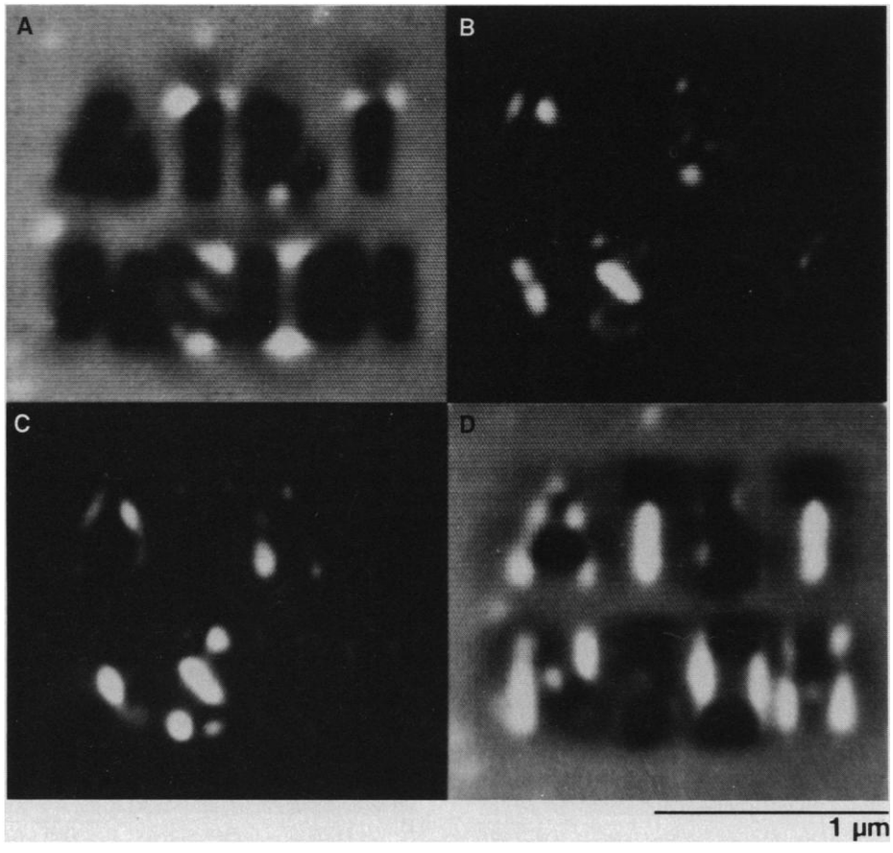

Fig. 4. Polarization contrast in NSOM as determined by various combinations of probe and detector polarization states: (**A**) probe |, detector |; (**B**) probe |, detector −; (**C**) probe −, detector |; (**D**) probe −, detector −.

REFERENCES AND NOTES

1. E. C. Teague, Ed., *Scanning Microscopy Technology and Applications*, SPIE vol. 897 (Society of Photo-Optical Instrumentation Engineering, Bellingham, 1988).
2. J. W. Goodman, *Introduction to Fourier Optics* (McGraw-Hill, New York, 1968).
3. G. A. Massey, *Appl. Opt.* **23**, 658 (1984).
4. E. H. Synge, *Phil. Mag.* **6**, 356 (1928).
5. E. A. Ash and G. Nicholls, *Nature* **237**, 510 (1972).
6. A. Lewis, M. Isaacson, A. Harootunian, A. Muray, *Ultramicroscopy* **13**, 227 (1984).
7. D. W. Pohl, W. Denk, M. Lanz, *Appl. Phys. Lett.* **44**, 651 (1984).
8. U. Ch. Fischer, *J. Vac. Sci. Technol. B* **3**, 386 (1985).
9. E. Betzig, A. Lewis, A. Harootunian, M. Isaacson, E. Kratschmer, *Biophys. J.* **49**, 269 (1986).
10. A. Harootunian, E. Betzig, M. Isaacson, A. Lewis, *Appl. Phys. Lett.* **49**, 674 (1986).
11. U. Durig, D. W. Pohl, F. Rohner, *J. Appl. Phys.* **59**, 3318 (1986).
12. E. Betzig, M. Isaacson, A. Lewis, *Appl. Phys. Lett.* **51**, 2088 (1987).
13. U. Ch. Fischer, U. T. Durig, D. W. Pohl, *ibid.* **52**, 249 (1988).
14. E. Betzig, thesis, Cornell University (1988).
15. D. W. Pohl, "Scanning near-field optical microscopy," in *Advances in Optical and Electron Microscopy*, C. J. R. Sheppard and T. Mulvey, Eds. (Academic Press, London, 1990).
16. E. Betzig, M. Isaacson, H. Barshatzky, A. Lewis, K. Lin, "Near-field Scanning optical microscopy," in (*1*).
17. H. A. Bethe, *Phys. Rev.* **66**, 163 (1944).
18. T. Wilson and C. Sheppard, *Theory and Practice of Scanning Optical Microscopy* (Academic Press, London, 1984).
19. K. Lieberman *et al.*, *Science* **247**, 59 (1990).

20. We thank H. Hess and R. B. Robinson for many helpful discussions.

30 November 1990; accepted 5 February 1991